J Therm Anal Calorim (2018) 131:1213–1220
https://doi.org/10.1007/s10973-017-6540-9

Investigation into the characteristics of Na_2CO_3-catalyzed steam gasification for a high-aluminum coal char

Yongwei Wang[1,2] · Zhiqing Wang[2] · Jiejie Huang[2] · Yitian Fang[2]

Received: 24 April 2017 / Accepted: 13 June 2017 / Published online: 20 June 2017

Abstract The effect of Na_2CO_3 additive on the steam gasification characteristics of Sunjiahao (SJH) coal char was studied in the present paper. Na_2CO_3-catalyzed steam gasification of SJH char was carried out in a thermogravimetric analyzer to study the effect of Na_2CO_3 loading on the gasification reactivity and in a fixed-bed reactor to investigate the evolution of char structure and the transformation of Na_2CO_3. The comparison result of the reactivity of char impregnated with various Na_2CO_3 catalyst loading indicates that the saturation level of Na_2CO_3 loading is 35 mass%. The catalytic gasification residues were characterized by a N_2 adsorption (77 K) technique, laser Raman spectra, and X-ray diffraction patterns. The analyses results of the BET surface of the catalytic gasification residues at different carbon conversion suggest that the block of Na_2CO_3 catalyst may lead to the smaller BET surface area of the catalytic gasification residue than that of uncatalyzed gasification residual sample. Raman spectra analyses show that the amount of amorphous carbon structure decreased with the process of catalytic char gasification. The results of XRD reveal that Na_2CO_3 changes into the mixture of sodium aluminosilicates during steam gasification and turns into $NaAlSiO_4$ after complete gasification.

✉ Yongwei Wang
wgreat@126.com

[1] Key Laboratory of Coal Clean Conversion and Chemical Engineering Process, College of Chemistry and Chemical Engineering, Xinjiang University, Urumqi 830046, People's Republic of China

[2] State Key Laboratory of Coal Conversion, Institute of Coal Chemistry, Chinese Academy of Sciences, Taiyuan 030001, People's Republic of China

Keywords Steam gasification · Na_2CO_3 · High-aluminum coal char

Introduction

The oil shocks have brought about the change of the conventional energy consumption structure in the past century, which leads to the increase in the production and utilization of coal and natural gas [1]. Natural gas has been given preference because it has high conversion efficiency and efficient end-use technologies besides the convenience of transportation [2]. With the rising demand of natural gas, the catalytic gasification of coal and/or biomass has been paid much attention, which can convert solid fuels to synthetic or substitute natural gas (SNG) [2–5]. However, it is difficult to put into industrial application in a large scale for the catalytic gasification of biomass, owing to the limitation of season and region. Therefore, catalytic coal gasification will play a significant role in SNG supply. In contrast to the traditional coal gasification technologies [6–8], catalytic coal gasification has outstanding advantages, such as low gasification temperature [9, 10], high gasification efficiency [11–13], and high methane production [2, 14]. Thus, catalytic coal gasification is a promising gasification technology.

The preferred catalysts for coal gasification reactions are the alkali and alkaline earth metals (AAEM), among which K_2CO_3 is the most efficient gasification catalyst [15–17]. Literatures reported that K_2CO_3 could efficiently improve the gasification reactivity of coal or char [18, 19]. To further enhance the catalytic activity of alkali carbonate, Sheth et al. [20, 21] investigated the catalytic performance of binary and ternary eutectic alkali carbonates for coal gasification, and found that the gasification rates of coal in

steam in the temperature range 923–1055 K could be substantially enhanced by adding binary or ternary eutectic alkali salt catalysts. They assumed that the reduced melting points of the eutectics could probably bring about the improvement of the catalytic activity at the lower gasification temperatures by achieving a better dispersion of the salt phases on the carbonaceous substrates. However, K_2CO_3 is easily react with the mineral matter in coal, giving rise to its deactivation [22, 23] and low recovery efficiency which may elevate the cost of gasification catalyst. It is well known that Na_2CO_3 is not only cheaper in price but also more abundant in reserves than K_2CO_3. Hence, Na_2CO_3 may be superior to K_2CO_3 for the catalytic coal gasification.

It is generally believed that the most appropriate reactor for catalytic coal gasification is a fluidized bed reactor [3, 24]. The addition of alkali catalyst during gasification will increase slagging risk. Therefore, the coals with high ash fusion point, such as high-aluminum coal, may be the candidate for the fluidized bed catalytic coal gasification. However, high-aluminum coals contain rich alumina which may react to the alkali catalyst to form water-insoluble aluminosilicate in the catalytic coal gasification, leading to the deactivation of catalyst [22, 23]. If some alumina can be extracted from the catalytic gasification residue of the high-aluminum coal during the recovery of the gasification catalyst, the cost of the catalyst recovery may be lowered. Thus, much attention should be paid to investigating the catalytic gasification process of high-aluminum coals.

Although few publications [25, 26] reported the effect of Na_2CO_3 additive on the gasification reactivity of coal or char, the transformation of sodium catalyst during gasification, especially for high-aluminum coals, was seldom investigated. Therefore, in order to deeply understand the catalytic action of Na_2CO_3 during gasification, the catalytic steam gasification of SJH high-aluminum coal char was studied using a thermogravimetric analyzer (TG) and a fixed-bed reactor. It is expected that this study can provide some guidance for Na_2CO_3-catalyzed gasification of high-aluminum coals.

Experimental

Samples and reagents

SJH bituminous coal was sampled from Inner Mongolia. The coal sample was first pulverized and sieved to a particle size of less than 120 μm. Then the sample was dried in an oven at 378 K for 12 h and finally stored in a desiccator for further use. The anhydrous salt of sodium carbonate (99.8% purity) was purchased from Tianjin Hengxing Chem. Co., Inc. and used as received. The proximate and ultimate properties of SJH raw coal and SJH char are listed in Table 1. The ash compositions of SJH raw coal and SJH char are presented in Table 2.

Preparation of SJH char and catalyst loading

Both the detailed experimental methods of preparation of SJH char and the experimental procedure for catalyst loading are conducted according to our previous work [27].

Steam gasification

The procedures of steam gasification are stated in detail in our reported publication [27]. Briefly, a magnetic suspension thermogravimetric analyzer (Rubotherm, 2011-01,181-CHN), which could introduce steam to the reaction system, was applied to measure the gasification reactivity of the coal chars. In each test, a 10 mg char sample was loaded in a platinum pan (13 mm diameter, 2 mm height), heated at a

Table 1 Proximate and ultimate analyses of SJH coal and SJH char

Sample	Proximate analysis/mass$_{ad}$%				Ultimate analysis/mass$_{daf}$%				
	V	FC	A	M	C	H	N	S	O[a]
SJH coal	29.63	51.22	16.92	2.23	78.85	4.91	1.46	0.80	13.98
SJH char	2.38	77.07	20.10	0.45	94.42	0.92	1.30	0.76	2.60

ad air-dried basis, *daf* dry ash-free basis

[a] By difference

Table 2 Ash compositions of SJH coal and SJH char/mass%

Sample	SiO_2	Al_2O_3	Fe_2O_3	CaO	MgO	TiO_2	SO_3	K_2O	Na_2O	P_2O_5
SJH coal	36.29	46.34	6.38	2.61	2.18	3.57	0.45	0.42	0.76	0.03
SJH char	36.09	46.64	6.58	2.51	2.08	3.50	0.43	0.27	0.42	0.04

ramp of 20 °C min^{-1} to the desired temperature in a flow of N_2 (200 mL min^{-1}), and held for 30 min to stabilize the system. Then the gas was switched to steam to initiate the isotherm gasification at atmospheric pressure, and 60 vol.% steam (96 μL min^{-1}, diluted by N_2, total flow was 200 mL min^{-1}) was used. The experiments were repeated 3–4 times, and the error of the experiments was within ±1%.

The carbon conversion (X) was calculated using the following equation:

$$X = \frac{m_0 - m_t}{m_0 - m_\infty} \quad (1)$$

where m_0 represents the initial mass of the char sample before gasification, m_t indicates the instantaneous mass of the char sample at time t, and m_∞ is the final mass or the total mass of ash and catalyst.

A reactivity index ($R_{0.5}$) [28] is applied to compare the gasification reactivity of raw SJH char with SJH char-added Na_2CO_3 catalyst, which is defined as

$$R_{0.5} = \frac{0.5}{\tau_{0.5}} \quad (2)$$

where $\tau_{0.5}$ is the gasification time (min) taken to reach a carbon conversion of 50%.

Preparation of the catalytic steam gasification residue samples

The preparation of the catalytic steam gasification residue samples is carried out in accordance with our previous work [27]. The catalytic gasification residues of SJH char were prepared in a horizontal quartz tube reactor at 800 °C under steam atmosphere (60 vol%, diluted by N_2). The conditions for the residual char preparation were similar to that of TG (details illustrated in "Steam gasification" section). The detailed procedure is as follows. A 3 g char sample was loaded in a ceramic boat and pushed into the middle of the quartz tube. Then all the connected parts were sealed, and the quartz tube was heated at a ramp of 10 K min^{-1} to the preset temperature under N_2 (purity 99.99%) atmosphere. When the desired temperature reached, steam was introduced into the tube reactor by the steam generator to start gasification. The experiment was ended at the desired carbon conversion. Then pure N_2 was purged into the tube until the temperature dropped to room level. The gasification residues were collected and stored in a desiccator for further analyses.

Characterization methods

Proximate and ultimate analyses were carried out in terms of the Chinese National Standard GB/T 212-2008 and GB476-91, respectively. The ash composition of the raw coal and char samples was tested by an inductively coupled plasma unit (Thermo ICAP 6300, Thermo Fisher Scientific, USA). The X-ray diffraction (XRD) patterns of the catalytic steam gasification residues were achieved by an X-ray diffractometer (D8 Advance, Bruker, Germany) with Cu/Kα radiation (k = 1.54056 Å), a 30 kV tube voltage, a 15 mA tube current, and a step size of 4° min^{-1} speed was used from 2θ = 5°–90°. Micromeritics TriStar 3000 was applied to conduct N_2 adsorption to assess the pore structure of samples. The total surface areas of the catalytic gasification residues were calculated through the Brunauer–Emmett–Teller (BET) equation for N_2 at 77 K. Raman spectral analyses of the residual chars were carried out using a Renishaw inVia Raman spectrometer (Renishaw Ltd, UK). A microscope equipped with 50 lenses was used to focus the excitation laser beam (514.5-nm exciting line of a spectra physics Ar laser) on the sample and to collect the Raman signal in the backscattered direction. The laser power on the sample surface was controlled at about 1 mW. The diameter of the laser spot on the sample surface was about 1 μm, considerably larger than the size of carbon microcrystallite in the char.

Results and discussion

Effect of the gasification temperature

In order to understand the effect of gasification temperature on reactivity of SJH char, the catalytic steam gasification of SJH char impregnated with 10 mass% Na_2CO_3 was carried out on TG at 973, 1023, and 1073 K, respectively. Figure 1 shows the gasification temperature dependence of the reactivity of SJH char with 10 mass% Na_2CO_3. Gasification temperature has a remarkable effect on the reactivity of SJH char with Na_2CO_3, which indicates that the gasification reactivity is sensitive to gasification temperature. The references also found that gasification temperature had a significant effect on the reactivity of coal char in the temperature range of 873–1073 K [9, 10]. Given that the reactivity of SJH char-added Na_2CO_3 is poor in the temperature region of 973–1073 K due to the high content of aluminum in SJH char, and given that the melting point of Na_2CO_3 is 1124 K, therefore, 1073 K is selected as the gasification temperature in this study so as to obtain larger reactivity and minimize the volatilization of sodium catalyst.

Effect of Na_2CO_3 loading

For the purpose of investigating the effect of catalyst loading on SJH char reactivity, all the experiments were carried out at 1073 K. Figure 2 displays the reactivity

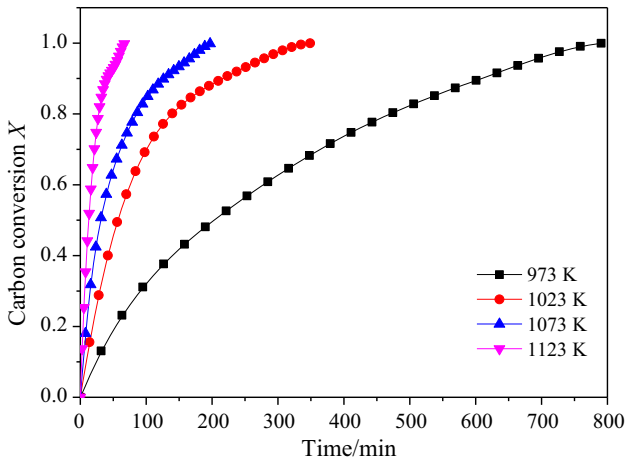

Fig. 1 Effect of temperature on the reactivity of SJH char with 10 mass% Na_2CO_3

results of SJH char impregnated with 0–40 mass% Na_2CO_3. It is apparent to see that the gasification reactivity increases with the increment in catalyst loading in the region of 0–35 mass%. However, the reactivity of SJH char with 40 mass% Na_2CO_3 is smaller than that of SJH char containing 35 mass% Na_2CO_3, which indicates that the loading saturation level of Na_2CO_3 may be reached for the catalytic steam gasification of SJH char at the catalyst loading of 35 mass%. The loading saturation level of Na_2CO_3 in this study was higher than the result reported by Li et al. [29] who pointed out that Na_2CO_3 showed saturation amount at 25 mass% for a gas coal catalytic gasification. Ding et al. [25] also investigated Na_2CO_3 catalyst loading on the Shenfu bituminous char reactivity and found that the saturation amount of Na_2CO_3 catalyst was between 10 and 15 mass%. However, Popa et al. [30] found that the saturation level of Na_2CO_3 loading is 3 mass% for the gasification of a Powder River Basin coal. The difference of the catalyst loading saturation level may be resulted from the difference of coal type and the gasification condition.

In order to investigate the degree of the effect of Na_2CO_3 loading on the gasification reactivity in detail, the reactivity index ($R_{0.5}$) is used to compare the gasification reactivity of raw SJH char with SJH char-added Na_2CO_3. The plot of reactivity index against catalyst loading increases monotonously from 0 to 35 mass% Na_2CO_3 loading, as can be seen from Fig. 3. Although the addition of 5 mass% Na_2CO_3 leads to an increase in 28% for $R_{0.5}$ of SJH char, the loading of 10 and 15 mass% Na_2CO_3 results in the substantial increase in $R_{0.5}$ of SJH char by 2.4 times and 33 times, respectively. When Na_2CO_3 loading reaches 35 mass%, $R_{0.5}$ increases 163 times unexpectedly. Therefore, Na_2CO_3 can remarkably improve the steam gasification reactivity of SJH char at 1073 K, especially beyond the loading of 15 mass%.

It is worthwhile to note that the gasification reactivity of SJH char loaded with 15 mass% Na_2CO_3 is by far larger than that of SJH char with 10 mass% Na_2CO_3. This sharp increase in the gasification reactivity may be related to the deactivation of catalyst. For SJH char with 10 mass% loading catalyst, most catalyst may be deactivated during the catalytic steam gasification, which leads to that the relative proportion of the active catalyst is remarkably lower than that of 15 mass% loading catalyst.

The BET results of the catalytic gasification char and residue samples

The measured results of BET surface areas by N_2 adsorption method are given in Table 3. As can be seen from the table, the BET surface area of SJH char with 10 mass% Na_2CO_3 is 9.6 $m^2\ g^{-1}$. Unexpectedly, the BET surface

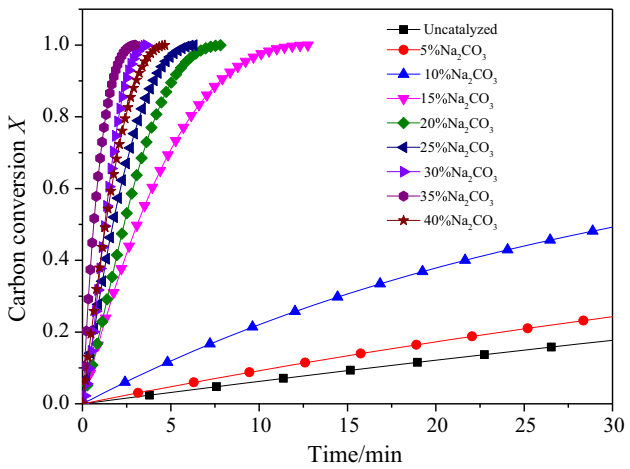

Fig. 2 Gasification reactivity comparison of SJH char with different catalyst loading

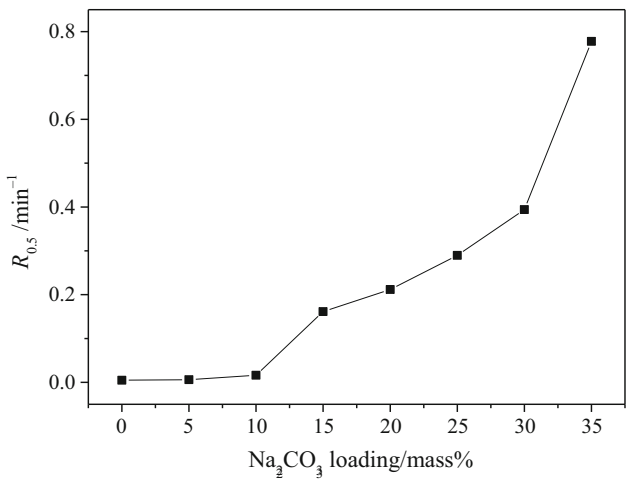

Fig. 3 Reactivity indexes of the catalytic steam gasification of SJH char obtained with different catalyst loading at 1073 K

Table 3 BET surface area of the gasification residues of SJH char impregnated with 10 mass% Na_2CO_3 and SJH char without catalyst at different carbon conversion

Catalytic gasification residues		Gasification residues without catalyst	
X/%	BET surface area/m^2 g^{-1}	*X*/%	BET surface area/m^2 g^{-1}
0	9.6	0	2.1
23.1	453.0	23.9	452.6
50.1	406.8	49.9	626.1

area of Na_2CO_3-catalyzed steam gasification residue of SJH char at 23.1% carbon conversion increases to 453 m^2 g^{-1}. This reveals that the BET surface area of SJH char increases with the proceeding gasification, which may be resulted from the predominance of the expansion of the micropore. Meanwhile, the BET surface area of uncatalyzed gasification residue of SJH char at 23.9% carbon conversion reaches 452.6 m^2 g^{-1}, which is similar to the BET surface area of catalyzed gasification residue at the corresponding carbon conversion. The nearly same BET surface area of catalyzed and uncatalyzed gasification residues indicates that the increment in the BET surface area may be resulted from the activation of steam rather than the effect of Na_2CO_3. However, the BET surface area of the gasification residue at 50.1% carbon conversion is smaller than that of the gasification residue at 23.1% carbon conversion, suggesting the dominance of the collapse of the micropore during gasification. In the case of uncatalyzed gasification, the BET surface area increases with carbon conversion. Therefore, the expansion of the micropore competes with the collapse of the micropore during the Na_2CO_3-catalyzed steam gasification. The variation trend of the micropore is also supported by the comparison result of the reactivity of SJH char with the conversion of fixed carbon during the course of the catalytic steam gasification.

In order to understand the reason of the BET surface area difference between the Na_2CO_3-catalyzed and uncatalyzed gasification residue, the BET results of the catalyzed gasification residue at 50.1% carbon conversion are compared with that of the same residue sample leached by water (listed in Table 4). Obviously, the BET surface area remarkably increases after water leaching, in contrast to the raw gasification residue. This shows that the smaller BET surface area of the catalyzed gasification residue may be caused by the block of Na_2CO_3, similar to the reported work [25].

Evolution of char structure during gasification

Raman spectroscopy is widely applied to characterize the structural features of carbonaceous materials [31–34]. In order to explore the evolution of SJH char structure during Na_2CO_3-catalyzed steam gasification, the residual char samples at different carbon conversion were characterized with laser Raman spectra. The recorded Raman spectra in the range between 800 and 1800 cm^{-1} were curve-fitted using the Origin 7.5 Peak Fitting Module, to resolve curve into ten Gaussian bands. The parameters including peak position, full width at half maximum, intensity, and integrated area of each band were accordingly derived. The spectral deconvolutions of the catalytic steam gasification residue samples are given in Fig. 4. Among the ten bands, the assignments of the five main bands (G, G_R, V_L, V_R, and D) are presented hereinafter according to the references [33, 35]. The G band at 1590 cm^{-1} originates from aromatic ring quadrant breathing. And the D (1300 cm^{-1}) band belongs to larger aromatic features with six or more fused rings, which represents medium-to-large-sized aromatic ring systems. The overlap between the D and G bands has been deconvoluted into three bands: G_R (1540 cm^{-1}), V_L (1465 cm^{-1}), and V_R (1380 cm^{-1}). These bands stand for typical structures in amorphous carbons (especially smaller aromatic ring systems) as well as the semicircle breathing of aromatic rings. And other five bands are deconvoluted to get a better curve fit. Therefore, only the five bands between 1300 and 1590 cm^{-1} (namely G, G_R, V_L, V_R, and D) will be used in this study.

Table 4 BET surface areas of the gasification residue of SJH char impregnated with 10 mass% Na_2CO_3 at the carbon conversion of 50.1% before and after water leaching

Sample	BET surface area/m^2 g^{-1}
Before water leaching	406.8
After water leaching	459.4

Previous work by the authors has shown that the intrinsic gasification reactivity of coal char can be influenced by char chemical structure as characterized by Raman spectroscopy [31, 32]. In order to observe the change of the char structure, the ratio of peak area is used to reflect the relative proportion of different band. I_G, I_D, and $I_{(G_R+V_L+V_R)}$ represent the peak area of the G band, the D band, and the total ($G_R + V_L + V_R$) band, respectively. The band area ratio $I_{(G_R+V_L+V_R)}/I_D$ is a useful indicator of impacts of process variables on char chemical structure from a reactivity perspective, as it gives a broad indication of the ratio of small to large (no less than six rings) aromatic ring systems. As shown in Fig. 5, the band area ratio of $I_{(G_R+V_L+V_R)}/I_D$ drops following the development of gasification. The decline of $I_{(G_R+V_L+V_R)}/I_D$ accounts for the reduction of the proportion of amorphous structures in coal char with the proceeding of gasification, which is consistent with the reported study [32]. The amorphous structures

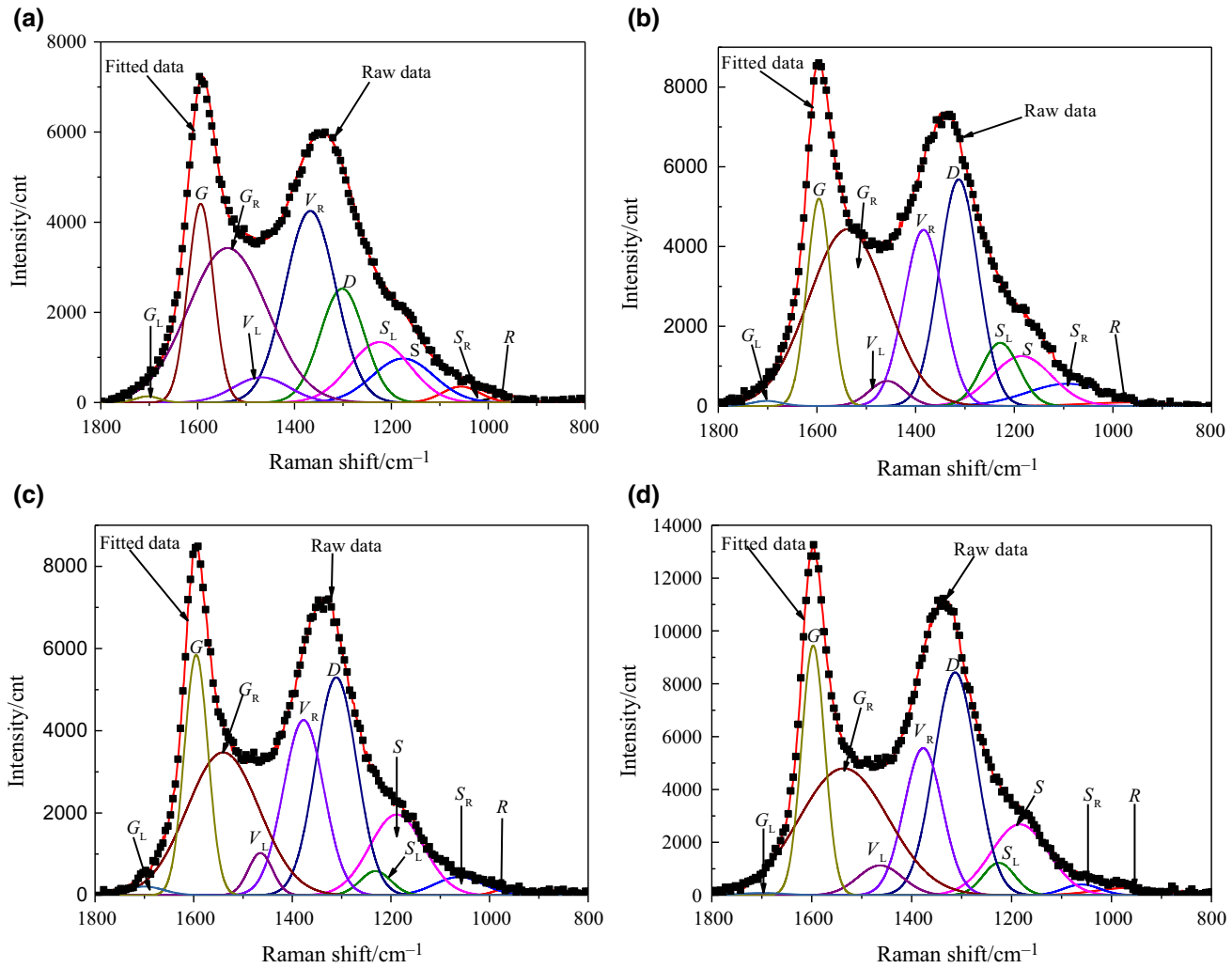

Fig. 4 Char samples of Raman spectrum fitted with ten bands. The char samples were prepared from Na_2CO_3-catalyzed steam gasification of SJH char at 1073 K for **a** before gasification; **b** 23.1%; **c** 47.9%; **d** 52.5%

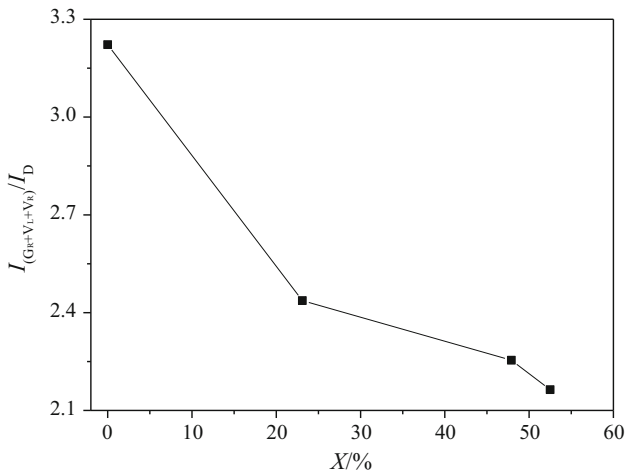

Fig. 5 Change in the ratio of $I_{(G_R+V_L+V_R)}/I_D$ during the catalytic steam gasification of SJH char at 1073 K

are related to the active sites during gasification. The decline of the amount of the amorphous structures may give rise to the decrease of the number of the active site, leading to that char reactivity becomes small with the consumption of the fixed carbon during the course of catalytic steam gasification. Therefore, the dropping tendency of gasification reactivity with carbon conversion shown in Figs. 1 and 2 is powerfully supported by the Raman spectra result.

XRD analyses of sodium forms during gasification

Figure 6 shows the XRD patterns of SJH char impregnated with 10 mass% Na_2CO_3 and the catalytic steam gasification residue samples at the carbon conversion of 23.1, 47.9, and 100%, respectively. As can be seen from Fig. 6a, only weak peaks assigned to Na_2CO_3 were found in the Na_2CO_3-impregnated SJH char. It is usually considered that

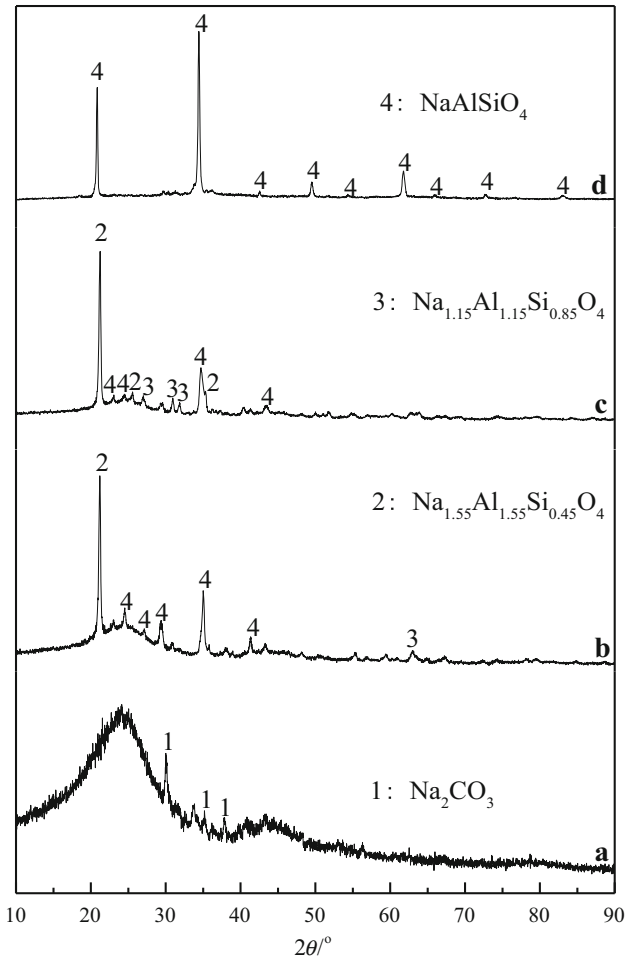

Fig. 6 XRD patterns of SJH char samples impregnated with 10 mass% Na_2CO_3 gasified at 1073 K **a** before gasification; **b** 23.1%; **c** 47.9%; **d** after complete gasification

coal char is composed of many basic structural units which contain condensed polynuclear aromatic and alkyl side chain/functional groups such as carboxyl and phenolic hydroxyl group. Part of Na_2CO_3 may be combined with the carboxyl and phenolic hydroxyl group in coal char, which is similar to the result reported by Zhang et al. [26]. As shown in Fig. 6, the sodium catalyst during steam gasification is mainly in the form of sodium aluminosilicate, and the composition of such sodium aluminosilicate changes with carbon conversion. The Na_2CO_3-catalyzed steam gasification residues of SJH char at 23.1 and 47.9% carbon conversion, according to Fig. 6b, c, mainly consist of $Na_{1.55}Al_{1.55}Si_{0.45}O_4$, $Na_{1.15}Al_{1.15}Si_{0.85}O_4$, and $NaAlSiO_4$, which is similar to the reported work by Mei et al. [36]. The sodium in the catalytic steam gasification ash, however, is only in the form of $NaAlSiO_4$ (shown in Fig. 6d). This is different from the conclusion drawn by Zhang et al. [26] who found that Na_2CO_3 transformed into $Na_6Al_4Si_4O_{17}$ instead of $NaAlSiO_4$ after complete gasification. This difference may be resulted from the different coal ash composition and different catalyst loading.

Conclusions

Through investigating the effect of Na_2CO_3 on the gasification behavior of SJH char during the catalytic steam gasification, the following conclusions have been drawn:

1. Na_2CO_3 can remarkably improve the steam gasification reactivity of SJH char at 1073 K, especially beyond the loading of 15 mass%.
2. The BET surface area of Na_2CO_3-catalyzed gasification residue becomes smaller than that of the uncatalyzed gasification residual sample, which results from the block of Na_2CO_3.
3. During Na_2CO_3-catalyzed gasification, the amount of the amorphous structure decreases with carbon conversion. The gasification reactivity of coal char has a close relationship with the char structure.
4. The sodium catalyst exists in the form of sodium aluminosilicate during the Na_2CO_3-catalyzed steam gasification of SJH high-aluminum char.

Acknowledgements The work is financially supported by the Strategic Priority Research Program of the Chinese Academy of Sciences (XDA07050100) and the Doctoral Research Foundation Project of Xinjiang University (BS160223).

References

1. Abas N, Kalair A, Khan N. Review of fossil fuels and future energy technologies. Futures. 2015;69:31–49.
2. Kopyscinski J, Schildhauer TJ, Biollaz SMA. Production of synthetic natural gas (SNG) from coal and dry biomass—a technology review from 1950 to 2009. Fuel. 2010;89:1763–83.
3. Nahas NC. Exxon catalytic coal gasif ication process. Fuel. 1983;62:238–40.
4. Gallagher JE, Euker CA. Catalytic coal gasification for SNG manufacture. Energy Res. 1980;4:137–47.
5. Sun Y, Zhang Z, Seetharaman S, Liu L, Wang X. Characteristics of low temperature biomass gasification and syngas release behavior using hot slag. RSC Adv. 2014;4:62105–14.
6. Yan Q, Huang J, Zhao J, Li C, Xia L, Fang Y. Investigation into the kinetics of pressurized steam gasification of chars with different coal ranks. J Therm Anal Calorim. 2013;116:519–27.
7. Zhao H, Cao Y, Orndorff W, Pan W. Gasification characteristics of coal char under CO_2 atmosphere. J Therm Anal Calorim. 2014;116:1267–72.
8. Kabir KB, Tahmasebi A, Bhattacharya S, Yu J. Intrinsic kinetics of CO_2 gasification of a Victorian coal char. J Therm Anal Calorim. 2015;123:1685–94.
9. Sharma A, Saito I, Toshimasa T. Catalytic steam gasification reactivity of HyperCoals produced from different rank of coals at 600–775 °C. Energy Fuels. 2008;22:3561–5.

10. Sharma A, Takanohashi T, Saito I. Effect of catalyst addition on gasification reactivity of HyperCoal and coal with steam at 775–700 °C. Fuel. 2008;87:2686–90.
11. Karimi A, Semagina N, Gray MR. Kinetics of catalytic steam gasification of bitumen coke. Fuel. 2011;90:1285–91.
12. Coetzee S, Neomagus HWJP, Bunt JR, Everson RC. Improved reactivity of large coal particles by K_2CO_3 addition during steam gasification. Fuel Process Technol. 2013;114:75–80.
13. Hu J, Liu L, Cui M, Wang J. Calcium-promoted catalytic activity of potassium carbonate for gasification of coal char: the synergistic effect unrelated to mineral matter in coal. Fuel. 2013;111:628–35.
14. Robert LH, Gallagher JE, Lessard RR, Wesselhoft RD. Catalytic coal gasification: an emerging technology. Science. 1982;215:121–7.
15. Wood BJ, Sancier KM. The mechanism of the catalytic gasification of coal char: a critical review. Catal R Sci Eng. 1984;26:233–79.
16. Nzihou A, Stanmore B, Sharrock P. A review of catalysts for the gasification of biomass char, with some reference to coal. Energy. 2013;58:305–17.
17. Leeuw KA, Strydom CA, Bunt JR, Niekerk D. The influence of K_2CO_3 and KCl on H_2 formation during heat treatment of an acid-treated inertinite-rich bituminous coal-char. J Therm Anal Calorim. 2016;126:905–12.
18. Kopyscinski J, Habibi R, Mims CA, Hill JM. K_2CO_3-Catalyzed CO_2 gasification of ash-free coal: kinetic study. Energy Fuels. 2013;27:4875–83.
19. Kopyscinski J, Rahman M, Gupta R, Mims CA, Hill JM. K_2CO_3 catalyzed CO_2 gasification of ash-free coal. Interactions of the catalyst with carbon in N_2 and CO_2 atmosphere. Fuel. 2014;117:1181–9.
20. Sheth A, Yeboah YD, Godavarty A, Xu Y, Agrawal PK. Catalytic gasification of coal using eutectic salts: reaction kinetics with binary and ternary eutectic catalysts. Fuel. 2003;82:305–17.
21. Sheth AC, Sastry C, Yeboah YD, Xu Y, Agarwal P. Catalytic gasification of coal using eutectic salts: reaction kinetics for hydrogasification using binary and ternary eutectic catalysts. Fuel. 2004;83:557–72.
22. Wang X, Zhu H, Wang X, Liu H, Wang F, Yu G. Transformation and reactivity of a potassium catalyst during coal-steam catalytic pyrolysis and gasification. Energy Technol. 2014;2:598–603.
23. Zhang J, Zhang L, Yang Z, Yan Y, Mao Y, Bi J. Effect of bauxite additives on ash sintering characteristics during the K_2CO_3-catalyzed steam gasification of lignite. RSC Adv. 2015;5:6720–7.
24. Sue-A-Quan TA, Watkinson AP, Gaikwad RP, Lira CJ, Ferris BR. Steam gasification in a pressurized spouted bed reactor. Fuel Process Technol. 1991;27:67–81.
25. Ding L, Zhou Z, Guo Q, Huo W, Yu G. Catalytic effects of Na_2CO_3 additive on coal pyrolysis and gasification. Fuel. 2015;142:134–44.
26. Zhang F, Xu D, Wang Y, Wang Y, Gao Y, Popa T, Fan M. Catalytic CO_2 gasification of a powder river basin coal. Fuel Process Technol. 2015;130:107–16.
27. Wang Y, Wang Z, Huang J, Fang Y. Catalytic gasification activity of Na_2CO_3 and comparison with K_2CO_3 for a high-aluminum coal char. Energy Fuels. 2015;29:6988–98.
28. Ye DP, Agnew JB, Zhang DK. Gasification of a South Australian low-rank coal with carbon dioxide and steam: kinetics and reactivity studies. Fuel. 1998;77:1209–19.
29. Li S, Cheng Y. Catalytic gasification of gas-coal char in CO_2. Fuel. 1995;74:456–8.
30. Popa T, Fan M, Argyle MD, Slimane RB, Bell DA, Towler BF. Catalytic gasification of a powder river basin coal. Fuel. 2013;103:161–70.
31. Wu H, Hayashi J, Chiba T, Takarada T, Li C. Volatilisation and catalytic effects of alkali and alkaline earth metallic species during the pyrolysis and gasification of Victorian brown coal. Part V. Combined effects of Na concentration and char structure on char reactivity. Fuel. 2004;83:23–30.
32. Guo X, Tay HL, Zhang S, Li C. Changes in char structure during the gasification of a Victorian brown coal in steam and oxygen at 800 °C. Energy Fuels. 2008;22:4034–8.
33. Wang M, Roberts DG, Kochanek MA, Harris DJ, Chang L, Li C. Raman spectroscopic investigations into links between intrinsic reactivity and char chemical structure. Energy Fuels. 2014;28:285–90.
34. Morga R, Jelonek I, Kruszewska K, Szulik W. Relationships between quality of coals, resulting cokes, and micro-Raman spectral characteristics of these cokes. Int J Coal Geol. 2015;144–145:130–7.
35. Li X, Hayashi J, Li C. FT-Raman spectroscopic study of the evolution of char structure during the pyrolysis of a Victorian brown coal. Fuel. 2006;85:1700–7.
36. Mei Y, Wang Z, Fang H, Wang Y, Huang J, Fang Y. Na-containing mineral transformation behaviors during Na_2CO_3-catalyzed CO_2 gasification of high-alumina coal. Energy Fuels. 2017;31:1235–42.